Ultra-Shallow Marine Anoxia in an Early Triassic Shallow-Marine Clastic Ramp (Spitsbergen) and the Suppression of Benthic Radiation

PAUL B. WIGNALL[1]*, DAVID P.G. BOND[2], YADONG SUN[3,4], STEPHEN E. GRASBY[5,6], BENOIT BEAUCHAMP[6], MICHAEL M. JOACHIMSKI[3] & DIERK P.G. BLOMEIER[7]

*corresponding author: p.wignall@see.leeds.ac.uk

[1]*School of Earth and Environment, University of Leeds, Leeds, LS2 9JT, United Kingdom.*

[2]*Department of Geography, Environment and Earth Sciences, University of Hull, Hull, HU6 7RX, United Kingdom.*

[3]*Geozentrum Nordbayen, Universität Erlangen-Nürnberg, Schlossgarten 5, 91054 Erlangen, Germany.*

[4]*State Key Laboratory of Biogeology and Environmental Geology, China University of Geosciences, 388 Lumo Road, Wuhan, 470073, Hubei Province, P.R. China.*

[5]*Geological Survey of Canada, 3303 33rd Street N.W., Calgary, Alberta, T2L 2A7, Canada*

[6]*Department of Geoscience, University of Calgary, 2500 University Dr. N.W., Calgary Alberta, T2N 1N4, Canada*

[7]*Millenia Stratigraphic Consultants, 35 Swansfield, Lechlade GL7 3SF, UK*

Abstract

Lower Triassic marine strata in Spitsbergen accumulated on a mid-to-high latitude ramp in which high-energy foreshore and shoreface facies passed offshore into sheet sandstones of probable hyperpycnite origin. More distal facies include siltstones, shales and dolomitic limestones. Carbon isotope chemostratigraphy compares allows improved age dating of the Boreal sections and shows a significant hiatus in the later Spathian. Two major deepening events, in the earliest Griesbachian and late Smithian are separated by shallowing-upwards trends that culminated in the Dienerian and Spathian substages. The redox record, revealed by changes in bioturbation, palaeoecology, pyrite framboid content and trace metal concentrations, shows anoxic phases alternating with intervals of better ventilation. Only the Dienerian-early Smithian witnessed persistent oxygenation that was sufficient to support a diverse benthic community. The most intensely anoxic, usually euxinic, conditions are best developed in offshore settings but at times euxinia also developed in upper offshore setting where it is even recorded in hyperpycnite and storm-origin sandstone beds; an extraordinary facet of Spitsbergen's record. The euxinic phases do not track relative water depth changes. For example, the continuous shallowing upwards from the Griesbachian to early Dienerian was witness to several euxinic phases separated by intervals of more oxic, bioturbated sediments. It is likely that the euxinia was controlled by climatic oscillations rather than intra-basinal factors. It remains to be seen if all the anoxic phases found in Spitsbergen are seen elsewhere although the wide spread of anoxic facies in the Smithian-Spathian boundary interval is clearly a global event.

1. Introduction

The development and intensification of marine anoxia during the Permian-Triassic is a well-known phenomenon widely regarded as a direct cause of the contemporary mass extinction (e.g. Wignall & Hallam, 1992; Isozaki, 1994; Wignall & Twitchett, 2002; Algeo *et al*. 2008; Bond & Wignall, 2010; Song *et al*. 2014). The subsequent Early Triassic interval saw widespread anoxia persist in shelf seas and oceanic waters (e.g. Isozaki, 1997; Wignall & Twitchett, 2002; Wignall *et al*. 2010). The consequent decrease of marine habitat area is thought to have been largely responsible for failure of benthic communities to recover and radiate in all but nearest shore settings where a narrow belt of oxygenated conditions persisted (Wignall, Morante & Newton, 1998; Beatty, Zonneveld & Henderson, 2008; Knaust, 2010; Zonneveld, Gingras & Beatty, 2010).

The temporal development and intensity of Early Triassic marine anoxia varied considerably with the Smithian/Spathian (S/S) interval being especially noteworthy as an intense phase of oxygen deprivation (Galfetti *et al*. 2007; Wignall *et al*. 2010; Meyer *et al*. 2012; Song *et al*. 2012; Grasby *et al*. 2013; Sun *et al.* 2015). However, other than studies in South China (e.g. Song *et al.* 2012; Tian *et al*. 2014) and the Sverdrup Basin (Grasby *et al.* 2013), the spatial development of marine anoxia is unconstrained and the context of the events, such as the S/S episode, within the prolonged history of the Early Triassic "superanoxic event" (*sensu* Isozaki, 1997), is poorly known. Here we aim to address this issue by establishing a depositional model for the Lower Triassic of Spitsbergen and then, using a combined ichnological/sedimentological/geochemical analysis, assess the temporal and spatial redox fluctuations in the region.

2. Regional Geology

The Lower Triassic succession in Spitsbergen forms a thick wedge of sediment peaking at ~ 500 m thickness in the westernmost outcrops at the entrance to Isfjorden and thinning to roughly half this thickness in more southerly and easterly outcrops on the island (Mørk, Knarud & Worsley, 1982). The thickest sections also display the most proximal facies and these are divided into the Vardebukta and Tvillingdodden formations that are roughly of Griesbachian-Dienerian and Smithian-Spathian ages respectively. Shales and siltstone dominate both formations but a major sandbody is developed in the upper part of the Vardebukta Formation in western outcrops (Nakrem & Mørk, 1991) that records shoreface and foreshore deposition (Wignall, Morante & Newton, 1998). The more eastern outcrops lack major sandstone beds and are instead dominated by shale and siltstone strata of the Vikinghøgda Formation (Mørk *et al.* 1999).

The Lower Triassic successions have been examined in detail at four locations:-

Festningen: This well-known coastal cliff section, at the western entrance to Isfjorden, provides a continuous exposure of the thickest-known development of Lower Triassic marine stratigraphy (Fig. 1). Only minor faulting in the lowest Tvillingdodden Formation and difficult-to-access sea cliffs in the uppermost part of the Formation hindered sampling.

Forkastningsdalen: This valley section lies at the western end of Nathorst Land in southern Spitsbergen (Fig. 1). The Upper Permian Kapp Starostin Formation is well exposed but the basal (presumably shale-dominated) part of the Vardebukta Formation is obscured. The outcrop resumes in streamside sections approximately 40 m stratigraphically above the highest Kapp Starostin outcrop and the ensuing 95 m-thick, sandstone-dominated succession is considered to belong to the upper Vardebukta Formation.

Tschermakfjellet: The basal metres of the Vikinghøgda Formation are exposed in a gully at Tschermakfjellet (Wignall, Morante & Newton, 1998; Dustira *et al*. 2013) but the overlying ~20 m is unexposed. The outcrop resumes a short distance to the south in coastal cliffs and reveals 56 m of section dominated by shales and siltstone with minor sandstone beds.

Vindodden: This steep hillside outcrop in eastern Sassenfjorden, lies below Botneheia Mountain. This is the type locality for the Middle Triassic Botneheia Formation and the phosphatic black shales of this unit are well seen in the cliffs above the softer-weathering shales of the Vikinghøgda Formation. Only the topmost 110 m of the Vikinghøgda Formation are seen and it can be correlated with the eponymous type location of this unit which lies ~15 km to the east of Vindodden. Comparison of sections between Vindodden and Vikinghøgda suggests a thinner development at the former locality. A distinctive, yellow-weathering, laminated dolostone with thin-shelled bivalves forms a distinct hillside ledge at both locations. At Vindodden this bed is 52 m below the Vikinghøgda/Botneheia boundary whereas it is recorded ~80 m below this contact at Vikinghøgda (Mørk *et al.* 1999).

3. Analytical Protocol

The four study sections were logged in detail and facies types were identified with care given to identifying body and trace fossils and semi-quantifying the intensity of bioturbation in all beds using the 5-point ichnofabric index (II) scheme of Droser and Bottjer (1986). Facies were determined in the field and further characterized by thin section analysis. In addition polished blocks from a range of facies were examined using backscatter scanning electron microscopy to determine their pyrite petrography and (where present) the size range of pyrite framboids (cf. Bond & Wignall, 2010).

Biostratigraphic control is available for the Vikinghøgda Formation at its type location and this allows the level of the S/S boundary to be estimated at the nearby Vindodden section. Samples were collected at this location and processed for conodonts in an attempt to further improve the biostratigraphic resolution. We employed three methods to disaggregate the samples. 1) samples were first treated with 10% acetic acid (buffered with tri-calcium phosphate) to remove carbonate contents; 2) samples were treated with 5% H_2O_2 for 3-5 times, and reaction between organic rich materials and H_2O_2 further disintegrated the samples; 3) finally samples were treated with industrial surfactant Rewoquat for two weeks to disaggregate phyllosilicates (see Jarochowska *et al.* (2013) for details). The residues of these processes were wet sieved, washed with distilled water and dried at 55 °C. Sodium polytungstate heavy solution (2.81 g/cm^3) was used for density separations. Conodonts were picked from the heavy fractions.

Early Triassic correlation can also be achieved using the $\delta^{13}C$ record, which shows substantial oscillations in this interval (Payne *et al*. 2004). Thus, detailed sampling was undertaken at Festningen and Vindodden and $\delta^{13}C_{org}$ values were generated. Stable isotope measurements were conducted at the Isotope Science Laboratory, University of Calgary and at GeoZentrum Nordbayern, University of Erlangen-Nuremberg. At Calgary, $\delta^{13}C$ was measured with a Finnigan Delta+XL mass spectrometer interfaced with a Costech 4010 elemental analyser. At Erlangen, $\delta^{13}C$ was determined with an elemental analyser (CE 1110) connected online to a ThermoFisher Delta V Plus mass spectrometer. All carbon isotope values are reported in the conventional δ-notation in permil relative to V-PDB (Vienna-PDB). Reproducibility of replicate standard analyses was ±0.07‰ (1σ, Erlangen) or ± 0.2‰ (1σ, Calgary).

A total of 180 shale beds of the Festningen section were sampled (by SEG and BB) for trace metal assay. Determination of molybdenum, uranium, and vanadium concentrations was performed at the Geological Survey of Canada. Elemental determinations were conducted on powdered samples digested in a 2:2:1:1 acid solution of H2O-HF-HClO4-HNO3, and subsequently analysed using a PerkinElmer mass spectrometer, with ± 2% analytical error.

4. Results

4.1. Chemo- and biostratigraphy

The $\delta^{13}C_{org}$ trends obtained at Festningen and Vindodden (Fig. 2) closely resemble the $\delta^{13}C_{carb}$ values from lower latitude Tethyan carbonate sections (Payne *et al.* 2004; Horacek *et al*. 2007) as well as the $\delta^{13}C_{org}$ record from the Smithian stratotype in the Sverdrup Basin (Grasby *et al.* 2013). This allows improved precision in age assignment for the Spitsbergen sections (Fig. 2).

At Festningen, the sharp negative excursion close to the base of the Vardebukta Formation is a marker for the Permian/Triassic boundary and this is followed by a rapid rise to heavier values (of -30 ‰) before a slowdown in the trend. The heaviest values are eventually attained around 200 m higher, in a sandstone unit. After this the $\delta^{13}C_{org}$ values begin a renewed fall that reaches a new low point 100 m higher in a shale-dominated section just above the Vardebukta/ Tvillingdodden formational boundary (Fig. 2).

Comparison with Tethyan records suggests that, following the Permian/Triassic boundary lowpoint, the slowdown in the rate of rise occurs within the Griesbachian Substage (Payne *et al*. 2004). A subsequent positive $\delta^{13}C$ peak occurs at the end of the Dienerian Substage in the Spitsbergen, Sverdrup Basin and China records (Grasby *et al.* 2013). The subsequent negative low point is at the end of the Smithian Substage and the remainder of the section (and nearly the entire Tvillingdodden Formation) therefore belongs to the Spathian Substage (Fig. 2).

These age assignments differ slightly from those suggested previously by Mørk *et al*. (1982) who placed the base of the Tvillingdodden Formation at the base of the Smithian, rather than in the mid Smithian as we suggest here (Fig. 2). The age of the eastern sections is also constrained by fossils, especially ammonoids, and is in much closer accord with the carbon isotope stratigraphy described above. Thus, the *Anwasatchites tardus* Zone straddles the S/S boundary (Mørk *et al.* 1999). No conodonts have been found from our Festningen samples but two thirds of samples from Vindodden yielded conodonts of which neogondolellids were the most common and indicate a Spathian age. *Neogondolella* sp A. (Orchard, 2008) occurs in the upper part of the section, indicating a middle Spathian age (*Subrobustus* ammonoid zone). *N. regalis* was found 104 m above the base of the Vindodden section and is a longlived form known to range from the middle Spathian to the early Middle Triassic. Smithian conodonts from the lower part of the section are rare. The conodonts are similar to those described by Dagis (1984) from Siberia and contrast starkly with coeval, low latitude faunas, which are dominated by *Neospathodus* species (e.g., Yan *et al.* 2013).

There is no conodont evidence for a latest Spathian age at Vindodden and comparison of $\delta^{13}C_{org}$ trends suggest that this interval may be missing beneath the base of the Botneheia Formation (Fig. 2). Thus, the $\delta^{13}C_{org}$ values in the Spathian strata at Festningen show an initial positive trend followed by a gradual ~2 ‰ negative shift around 370 m followed by stable values for 100 m before a final minor, positive trend in the uppermost 30 m of the Tvillingodden Formation. At Vindodden only the initial positive shift and the gradual negative shift (but not the prolonged stable phase) are seen above the S/S boundary (Fig. 2). This suggests that the upper part of the Spathian Stage has been removed by erosion (or the upper Spathian is highly condensed) at Vindodden. Further evidence for erosive removal comes from the basal bed of the overlying Botneheia Formation, which is an erosive-based sandstone with rounded phosphatic clasts. It is possible that a late Spathian hiatus occurs at Festningen too, albeit of briefer duration than that seen at Vindodden. The Sverdrup Basin and Tethyan records shows that a marked positive trend in the latest Spathian (of 4‰ amplitude in both organic and carbonate records): this trend is only weakly manifest at Festningen suggesting it has been truncated (Fig. 2).

4.2. Facies

The two western-most sections (Forkastningsdalen and Festningen) show the presence of a major sandbody in the upper Vardebukta Formation whereas, further to the east, only thin sandstone beds (<50 cm thickness) are present at Tschermakfjellet, and at Vindodden they are very rare and <20 cm thick. This progressive eastward loss of sandstone supports a proximal-to-distal, west-to-east transition found by previous workers (Mørk, Knarud & Worsley, 1982; Nakrem & Mørk, 1991; Wignall, Morante & Newton, 1998). Nine facies types are present in the sections:-

1. Swash cross-stratified sandstone: Medium sandstone with planar laminations that show very low angle truncation surfaces typical of swash cross stratification. Bioturbation intensity is low (II 2) and consists of vertical burrows (*Skolithos, Arenicolites* and *Diplocraterion*), which can penetrate downwards for ~50 cm. Examples of this facies type are only seen at two levels: near the top of the Forkastningsdalen section and, around the same stratigraphic level, ~ 200 m above the base of the Festningen section (cf. Wignall, Morante & Newton, 1998; Fig. 3). Desiccation cracks have been reported from *Skolithos*-bearing sandstone from around this level at Festningen (Mørk, Embry & Weitschat, 1989).

This facies type is interpreted to record foreshore conditions and is the shallowest-water facies seen in this study.

2. Sandy bioclastic grainstone: Limestone composed of thick-shelled bivalves and bryozoans arranged in tabular cross sets ~1m in height. Cross beds record multimodal current flow directions. Sand-grade abraded bone material and phosphatic pellets are common. Where identifiable, the bivalves mostly belong to

Promyalina, which have been recrystallized, and sometimes show slender borings (Fig. 4a). Prisms of calcite, present amongst the bioclastic debris, are probably from disintegrated valves of prismatic-shelled bivalves. Other fossils include echinoderms (probably ophiuroids) and bryozoans (*Paralioclema*). This facies is present in several beds at Forkstningsdalen (where they can be up to 2m thick), and at one level at Festningen.

The sedimentology of this facies indicates persistent high-energy conditions (as testified by the abraded phosphatic debris) in a shoreface setting with dune-scale bedforms recording variable flow directions.

3. Cross-bedded sandstone: Medium grained sandstone displaying trough cross sets varying from 0.2 – 0.6 m in height seen at Festningen and Forkastningsdalen. As with Facies 2 palaeocurrents vary although stacks of cross sets with consistent dip are common (Wignall, Morante & Newton, 1998). Glauconite and phosphatic sand grains are present and the bottom sets can contain a lag of prismatic-shelled bivalve and brachiopod fragments together with small phosphatic concretions.

As with Facies 2 cross-bedded sandstone are considered to be the product of fairweather processes in a shoreface although the smaller dune height suggests a deeper setting.

4. Hummocky cross-stratified (HCS) sandstone: Fine-grained sandstone showing the characteristic HCS-style thickening of laminae above erosive lowpoints to produce hummocks. Generally found in thin sandstone beds (~ 10 cm thick) the hummocks range from <20cm in width to a few centimetres (Fig. 4b). Fine sand-

grade pyrite grains are a common component. This very rare facies type is seen in a few beds at Festningen where it is interbedded with facies 7.

HCS bedforms are generally considered the product of storm wave conditions (Dumas & Arnott, 2006). If this is the case with the Festningen examples then storms were rare in the Early Triassic of Spitsbergen.

5. Sheet sandstone: This common facies type consists of thin sheets of fine and medium-grained sandstone separated by siltstone beds (Fig. 5a). Individual beds range from 2 – 80 cm thick and can be stacked to produce composite beds up to 2 m thick that show little or no erosion at the bed boundaries. Internally, they commonly show fluctuating grain size with mud laminae intercalated with silt and fine sand laminae. Occasionally flute marks and small flame structures occur on the base of beds. Most beds are either planar laminated, current-ripple laminated or wave rippled (Fig. 4c). The thicker beds often appear structureless but many are current-rippled on careful inspection and the thickest individual beds commonly show climbing ripple lamination recording flow was consistently offshore (eastwards). In contrast the wave-rippled beds rarely exceed 10 cm in thickness. Often beds show alternations of planar laminated and current-rippled parts and thicker beds may show a vertical succession from planar lamination, to current ripple lamination to wave-rippled top surfaces.

Quartz grains dominate the mineralogy but pyrite and glauconite grains can also be common (Fig. 4c). Fossils are locally common and dominated by examples of *Promyalina* and *Claraia*. Bioturbation varies in intensity (discussed below) and typically consists of burrows that either penetrate the top surface (e.g. *Monocraterion*) or cut the entire bed (e.g. chevron escape traces).

Sheet sandstone records rapid deposition as indicated by the loading, escape traces and climbing ripple sets. Flows were only occasionally strong enough to erode the substrate prior to deposition (as shown by the presence of rare flutes) but the general lack of bed amalgamation indicates a deposition-dominated regime. In some regards the sheet sandstone facies resemble the product of decelerating turbidity currents but the frequent wave rippling does not fit this origin. Also, unlike typical turbidite systems there is no evidence for any organized stacking patterns typical of turbidite lobes (e.g. Macdonald *et al.* 2011) and neither are submarine channels apparent.

A storm deposition origin is possible for this facies, but typical storm bed attributes such as gutter fills and multimodal tool marks are absent whilst HCS (Facies 4) is very rare. Arnott (1993) has described quasi-planar-laminated sheet sandstone beds often with current-rippled tops from lower shoreface/inner shelf environments. He attributes these beds to a storms in which an initial high-velocity, oscillatory upper flow regime produces near-flat laminae and is followed by waning unidirectional flow recorded by ripples. This rather atypical storm facies fits some of the attributes of the sheet sandstone facies of Spitsbergen although there is a much greater abundance of wave rippling than in Arnott's (1993) example.

River-fed hyperpycnites show many of the attributes of this sheet sandstone facies. These include sheet geometry and common planar and current ripple although they lack an initial coarsening-upwards component that records surging discharge (Mulder *et al*. 2003; Plink-Björklund & Steel, 2004). However, they do show common clay laminae interbedded with fine sandstones suggesting fluctuating discharge during bed deposition (Fig. 4c).

6. Wrinkle-Laminated Sandstone: This facies is only seen at Forkastningsdalen in laminated beds of sandstone 20-30 cm thick interbedded with facies 5 (Fig. 5b). Such structures are common in both the Precambrian and the Early Triassic and show a range of linearity (e.g. Pruss, Fraiser & Bottjer, 2004). The Spitsbergen examples consist of flat-topped parallel ridges and grooves of millimetre heights that extend through many laminae. Bioturbation by *Planolites* and short, vertical burrows is common but not intense (II 2).

Wrinkle structures are thought to form from microbial binding of sediment in shallow-marine settings (Pruss, Fraiser & Bottjer, 2004).

7. Siltstone: Beds of laminated siltstone are found in all locations and range from 1 – 20 cm thickness. The laminae are composed of weakly graded layers of quartz silt that often show concentrations of silt-grade pyrite grains at their base (Fig. 4d). Bioturbation intensity is highly variable and can reach II 6 (Fig. 5d). Only at Forkastningsdalen does the fossil content become significant, consisting of thin-valved, prismatic-shelled bivalves. At this location there is also a unique bed of highly bioturbated (II6) siltstone that contains an abundant fauna dominated by bryozoans (*Paracliolema*), echinoderm grains (mostly ophiuroid material), *Promyalina* and spirorbids (Fig. 6).

The graded laminae of the siltstones suggest that this facies it is part of a continuum of event bed-style deposition that includes the sheet sandstone facies. Benthic oxygenation clearly varied greatly from the well-oxygenated conditions of the thoroughly-bioturbated, bryozoan bed to the more common, unbioturbated beds of laminated, pyritic siltstone.

8. Shale: Shale beds typically display fine lamination, consisting of alternations of silt-rich and clay-rich laminae that are sometimes partially or completely destroyed by bioturbation. Carbonate concretions are locally common. The thickest shale unit at Festningen occurs between at 275 - 310 m above the base of the Vardebukta Formation and it straddles the Smithian/Spathian boundary whilst at Vindodden the majority of the section is composed of shale.

The shale beds record low energy conditions in which the silt-rich laminae are probably deposited from weak traction currents. The variation from undisturbed lamination to intense bioturbation suggests oxygen levels varied considerably in this basinal facies.

9. Laminated dolomite: Rare cementstone horizons, composed of silt-grade dolomite rhombs, occur interbedded amongst the shales at Vindodden. The thickest example is found 56 m above the base of the section where a 2 m-thick bed of yellow, laminated dolostone with common "*Posidonia*" bivalves is found (Fig. 5c). Thin section shows organic-rich laminae and abundant pyrite grains. Small microspheres are also present, which are possibly recrystallized radiolarians.

The laminated dolomite is an anoxic-dysoxic, hemipelagic facies possibly with a significant "pelagic rain" of radiolarians, although substantial dolomitisation has obliterated details of the fabric.

4.3. Bioturbation Intensity

The intensity of bioturbation varies substantially in all sections (Figs. 3, 5d, 7). Diversity of ichnogenera is modest and dominated by *Thalassinoides*, *Planolites* and *Diplocraterion* (Wignall, Morante & Newton, 1998). Burrow depths rarely exceed more than a few centimetres except in facies 1 where it can be more than 50 cm.

Fully bioturbated levels (II 6) occur at a level in the Dienerian of Festningen and in the bryozoan bed (probably also of Dienerian age) at Forkstningsdalen (Fig. 7). Both levels are also associated with peaks of benthic diversity in their respective sections. The fauna of the bryozoan bed fauna is noted above and the Festningen bioturbated horizon contains *Promyalina*, *Unionites*, *Claraia*, microgastropods, ophiuroids and brachiopods.

Perhaps surprisingly, there is little facies control to the laminated levels; only facies 1 and 6 are consistently bioturbated, whilst facies 2 and 3 are rarely bioturbated probably because a shifting substrate of dunes was difficult to colonize by mobile infauna. The other facies types occur as both burrowed and unburrowed varieties. Often the transition between burrowed/unburrowed strata is very sharp, occurring over a few centimetres, and is developed within a consistent facies type.

4.4. Framboid petrography

Pyrite grains and framboids are common in the Lower Triassic strata of Spitsbergen and occur both in fine-grained facies and the sheet sandstone. At most levels the framboids are of small diameter and show little size variation – a distribution typical of framboid populations from modern euxinic settings (Fig. 8). Larger, more variable framboids populations occur in some of the bioturbated intervals although they still fall within the dysoxic field when compared to framboids produced in modern environments (Wilkin, Barnes &

Brantley, 1996). Framboids only become consistently rare/absent in the shoreface and foreshore sediments (facies 1-3) and in the fully bioturbated, high diversity Dienerian strata noted above.

4.5. Trace metals

Analysis of the redox-sensitive trace metals uranium, molybdenum and vanadium at Festningen revealed two distinct trends. Uranium and vanadium show high concentrations (around 2 ppm and 50 ppm respectively) and high U/Al and V/Al ratios through most of the Early Triassic (Fig. 9). Somewhat higher uranium values (≤ 5 ppm) are also encountered in the shale-dominated Smithian/Spathian boundary interval. In contrast, the behaviour of molybdenum is fundamentally different. Following an initial peak in the P/T boundary interval, Mo is not enriched (< 1 ppm) and the Mo/Al ratio remains around 0 in the Vardebukta Formation. Mo concentrations then exhibits highly variable values (<1 – 10 ppm) and Mo/Al ratios above the S/S boundary (Fig. 9).

5. Discussion

5.1. Depositional Model

The proximal-distal trend in the Early Triassic successions of Spitsbergen envisages nearest-shore conditions in the sandstone-rich western-most outcrops passing distally to the east where the shale-dominated sections are found (Mørk, Knarud & Worsley, 1982; Wignall, Morante & Newton, 1998). This transition allows a facies model to be constructed in which high energy foreshore and shoreface facies pass offshore into the hyperpycnite sand sheets of facies 5 (Fig. 10). These sheets were presumably river fed although there is no record of fluvial conditions in the succession. Other potential origins for facies 5 include storm deposition (e.g. beds showing HCS), but the evidence is rare. A shoreface-attached turbidite system seems unlikely due to the lack of organisation of the sheets. It is noteworthy that the most distal development of the sheet sandstone beds, seen at Tschermakfjellet, are wave-rippled indicating that water depths were still shallow enough for wave influence even though this location is >50 km offshore from the contemporaneous shoreface at Festningen. Shale and siltstone beds that are mostly finely laminated dominate the most offshore setting.

The vertical succession of facies consists of two long-term cycles. Following a major transgression at the start of the Griesbachian, shale facies are developed throughout the region, this is followed by a shallowing/progradation trend that lead to the establishment of shoreface/foreshore sandstones in westerly outcrops during the Dienerian. Gradual deepening during the following Smithian culminated in widespread shale deposition once again around the Smithian/Spathian boundary. The succeeding Spathian succession records shallowing although the trend only culminates in facies 5 at Festningen; the Dienerian littoral facies (Facies 1-3), are not repeated. Base level fall may also have eroded and removed upper Spathian strata at Vindodden.

5.2. Redox Trends and Shallow Marine Anoxia

The lack of bioturbation and benthic fossils in multiple levels of the Lower Triassic succession of Spitsbergen suggests intensely anoxic/euxinic depositional conditions. This interpretation is supported by elevated trace metal concentrations (of U and V) and the size range of pyrite framboid populations that points to a sulphidic lower water column (Figs. 8 & 9). However, burrowed strata are also present indicating improved ventilation and the associated framboid populations further indicate dysoxic bottom waters at these levels. Thus, the Early Triassic redox record can be divided into phases of euxinia (labelled I to XI in Figure 3) separated by dysoxic/oxic phases. The best oxygenated strata (II 6, diverse benthos, no framboids) occur in the Dienerian.

Unfortunately it is not possible to confidently correlate the redox cycles between sections due to insufficient stratigraphic resolution (further $\delta^{13}C$ study of all sections is needed). However, it seems likely that euxinic phases III and IV at Festningen are also seen at Forkastningsdalen because they occur around the same level (Fig. 3). Phases V to VIII at Festningen are separated by thin intervals of dysoxic strata whilst further offshore at Vindodden a similar number of euxinic/dysoxic alternations is seen. If it is assumed that the upper part of the Spathian is not present at Vindodden (see discussion in "Chemo- and Biostratigraphy" above) then it becomes possible to correlate the anoxic phases between locations. Thus phase XI becomes the highest phase at Vindodden (Fig. 3).

The most extraordinary facet of the Early Triassic euxinic episodes is their development in exceptionally shallow-water settings. Many of the sheet sandstones, interpreted as hyperpycnites formed in upper offshore setting (Fig. 10), lack burrows and benthic fossils but possess framboids characteristic of euxinic deposition. The shale interbeds amongst the sandstone beds also show trace metal enrichment suggesting anoxic conditions. Typically, examples of nearshore-restricted euxinic black shales are considered to form in sheltered bottom waters beneath a pycnocline during base-level rise (e.g. Wignall & Newton, 2001). However, the Spitsbergen shallow-water euxinic facies are lithologically much more diverse than black shale facies and they differ significantly from other transgressive, anoxic facies because the Spitsbergen anoxic phases show little relationship to base-level changes. For example, the prolonged single episode of shallowing-up that spans the Griesbachian to late Dienerian stages is associated with four euxinic phases developed in successively shallower waters.

As a final observation, it is noteworthy that the $\delta^{13}C_{org}$ curve closely matches that found in Tethyan carbonates. This is despite the fact that it is obtained from a clastic and frequently nearshore environment. Such a setting, with high terrigenous run off, might be expected to show more "noise" caused by the mixing of variable amounts of marine and terrestrial organic carbon. That it does not suggests a uniform source perhaps dominated solely by marine organic matter. The Early Triassic is noteworthy for its global "coal gap" (Retallack, Veevers & Morante, 1996), and it may have been the case that there was little terrestrial organic productivity at this time. However, in a noteworthy counterpoint, it has been suggested that woody vegetation biomass recovered after the S/S boundary (Saito *et al*. 2013).

5.3. Global Early Triassic Redox

The generally poor level of ventilation in Early Triassic shallow seas of Spitsbergen may have its origin in high oxygen demand, fostered by high productivity at a time of high runoff (e.g. Algeo & Twitchett, 2010). However, the phases of anoxia are not related to proximity to terrestrial nutrient supply nor to water depth suggesting another factor is more important. The anoxic phases correspond to the sea-surface temperature (SST) record of Sun *et al*. (2012). It is especially noteworthy that the two Early Triassic peaks of SST, in the Griesbachian and late Smithian, coincide with intervals of prolonged and extensive euxinia in Spitsbergen (Fig. 11). In contrast, the Dienerian Substage is the coolest interval of the Early Triassic SST curve and also the best-oxygenated period in Spitsbergen, and also globally (Wignall & Twitchett, 2002). There are three causal links between high temperatures and anoxia that may be at play here:-

i) dissolved oxygen levels decline with temperature.
ii) organic matter remineralisation rates increase with temperature thereby increasing oxygen demand within the water column.
iii) a general link between warmer climates and increased humidity, thereby increasing nutrient run-off to the oceans.

If global temperature is a key factor in the Spitsbergen euxinic phases then it suggests such conditions should have been widespread. The Early Triassic is indeed known as a “superanoxic episode” characterized by widespread ocean anoxia (Isozaki, 1997) and recent work has demonstrated detailed fluctuations within this generally poorly ventilated oceanic interval (e.g. Wignall *et al.* 2010; Grasby *et al*. 2013; Tian *et al.* 2014). Anoxia was especially widespread during the Griesbachian, the S/S boundary interval and the late Spathian – all intervals of euxinia in Spitsbergen. Further work is needed to test whether these Spitsbergen euxinic phases are global cycles or regional ones.

The concept of widespread Early Triassic anoxia has however been challenged. Resurrecting an original idea of Erwin (1993), Hofmann *et al*. (2015, p.9) suggest that the prevalence of laminated sediment was caused by "extinction [at the end of the Permian], rather than the environmental exclusion, of bioturbators", producing an Early Triassic world with no animals capable of generating thoroughly bioturbated surficial sediments. This is suggested to have caused intense anoxia within the sediment producing a geochemical signal that reflects this. The Spitsbergen record clearly shows this scenario is untenable because it consists of alternations of laminated and intensely bioturbated strata. Intense burrowing is also known from other regions (e.g. Beatty, Zonneveld & Henderson, 2008; Zonneveld, Gingras & Beatty, 2010), and even Hofmann himself records intense bioturbation (ii 4) from the Lower Triassic of Italy (Hofmann *et al.* 2011). Early Triassic bioturbators were readily capable of generating thoroughly mixed sediments but "environmental exclusion" was common and the available evidence overwhelmingly favours anoxia as a cause.

6. Conclusions

A new $\delta^{13}C_{org}$ record from Spitsbergen, together with sporadic conodont finds, allows a major improvement in age dating of the Spitsbergen succession. The Early Triassic record is seen to consist of hyperpycnite sandstone and shale dominated ramp facies. Shoreward these pass into shoreface facies displaying shell-rich, cross-bedded strata and foreshore facies. Relative water depth changes saw deepest-water conditions in the earliest Griesbachian and around the Smithian/Spathian boundary with shallowest waters in the late Dienerian. Regression in the later Spathian may be responsible for the truncation of Spathian strata in the region.

Much of the Lower Triassic strata accumulated in oxygen-poor and frequently euxinic waters, including hyperpycnite sand sheets, and points to intervals of exceptionally shallow-water development of such conditions. However, the anoxic phases, of which at least a dozen are developed, do not correlate closely with water depth changes. Instead, there may have been a climatic control on the Early Triassic anoxic phases with the most intense anoxia developed at times of greatest warmth. The best oxygenated Early Triassic interval occurred during the coolest phase, in the earliest Dienerian, and was witness to the development of a highly diverse benthic community found in thoroughly bioturbated sediments.

Acknowledgements

This research was funded by NERC grants NE/I015817/1 (to PW), and NE/J01799X/1 to D. Bond), and by the Research Executive Agency (Marie Curie Intra-European Fellowship FP7-PEOPLE-2011-IEF-300455 to D. Bond). We thank the Norwegian Polar Institute, and in particular Jørn Dybdahl and Monica Sund, for logistical support in the field, Jason Hilton, Thomas Wignall, Tom Goode, Christian Scheibner and Dan Collins for field assistance and Sara Pruss for helpful discussions. Christian Bjerrum and anonymous reviewer provided useful comments on an earlier version of the manuscript.

Figure captions

1. Map of Spitsbergen within the Svalbard archipelago, showing the locations of studied sections.

2. Correlation of the Festningen and Vindodden sections based on their $\delta^{13}C_{org}$ trends. Stage boundaries are derived by comparing with the similar $\delta^{13}C_{carb}$ record from conodont-dated sections in South China (Payne *et al*. 2004; Horacek *et al*. 2007) and the Smith Creek $\delta^{13}C_{org}$ record of the Sverdrup Basin (Grasby *et al.* 2013). Aeg. = Aegian Substage; Bot. = Botneheia Formation.

3. Correlation of Lower Triassic successions in Spitsbergen, thicknesses in metres. Stage-level age assignments are based on $\delta^{13}C_{org}$ chemostratigraphy supported by fossil evidence from conodonts and ammonoids. The grey-and-white "barcodes" adjacent to the lithological columns distinguish between bioturbated and unbioturbated/laminated phases. These have been labelled (I – XI) at Festningen for ease of description in the text. Anoxic phases occur in the other sections but it is uncertain if these levels can be correlated.

4. Photomicrographs of: a) facies 2 at Forkastningsdalen showing a boring in thick-shelled bivalve (labelled x), in which the shell is replaced with a blocky mosaic of calcite crystals, and bryozoans (*Paralioclema*) (labelled y). Field of view is 20 mm wide. b) facies 4 Festningen, upper Vardebukta Formation showing small-scale hummocky cross stratification. Field of view is 32 mm wide. c) facies 5, showing, in the lower half of the section, initial ripple cross lamination, overlain by planar laminated sandstone and a mud lamina. The upper half of the section is planar laminated sandstone. Basal Tvillingdodden Formation, anoxic phase VII, Festningen. Field of view is 35 mm wide. d) graded silt laminae (facies 7) showing concentration of pyrite (opaque grains) in the

lower part of the field of view. Anoxic phase IV, Vardebukta Formation, Festningen. Field of view is 1.3 mm wide.

5. Field photographs. a) Sheet sandstone beds ~ 10 cm thick, interbedded with shale and siltstone from a level 265 m above the base of the Vardebukta Formation at Festningen; b) Wrinkle structures, showing wrinkles present on numerous bedding planes. Forkstningsdalen. Occasional, short vertical burrows cut through the laminae (e.g. left of pencil tip); c) laminated shale and dolomite found around the Smithian/Spathian boundary at Vindodden. Total height of field of view is ~ 2 m; d) bioturbated silty mudstone (facies 8) from the Smithian at Festningen (between anoxic phases V and VI).

6. Photomicrograph of a bryozoan-rich bed, Vardebukta Formation, Forkstningsdalen showing bryozoans (b), spirorbids (s), ophiuoroid elements (o), and bivalves (c) in a siltstone matrix. Field of view is 1.5 mm wide.

7. Detailed logs of the Festningen section (from 70 – 120 m) and the Forkastningsdalen section (from 40 – 90 m) showing fluctuations in ichnofabric index used to define the anoxic phases. Peak diversity occurs in the bioturbated strata between anoxic phases III and IV where bryozoans and bivalves are common. The laminated beds are generally unfossiliferous except for levels where *Promyalina* occurs.

8. Mean versus standard deviation plot of framboids populations (>100/sample) from Lower Triassic samples of Spitsbergen. The redox-related fields are derived

from size-frequency distributions of framboids from modern euxinic, anoxic and dysoxic settings (cf. Wilkin *et al.* (1996) and Bond & Wignall (2010)) and reveals that many of the Spitsbergen samples formed in euxinic waters. No framboids occurred in the highly bioturbated (II ≥ 4) samples we examined.

9. Carbon isotope and trace metal data from Festningen. Our two $\delta^{13}C_{org}$ records are in close accord (black circles, curve generated in Calgary; open triangles, curve generated in Erlangen). The concentrations of the redox-sensitive trace metals Mo, U, and V have been normalised to Al.

10. Depositional model for the Lower Triassic shallow-marine strata of Spitsbergen showing location of facies described in the text. FWWB – fairweather wave base, SWB – storm wave base.

11. Correlation of Spitsbergen anoxic phases with the sea surface temperature (SST) record of Sun *et al*. (2012). The width of the SST curve denotes the minimum and maximum SSTs based on conodont apatite oxygen isotopes. A ~2°C warmer record was obtained around the Smithian/Spathian boundary from surface-dwelling conodonts. There is a correspondence between the warmest phases in the Griesbachian and Smithian and the frequent development of anoxic phases.

References

Algeo, T.J., Shen, Y., Zhang, T., Lyons, T., Bates, S., Rowe, H. & Nguyen, T.K.T. 2008. Association of ^{34}S-depleted pyrite layers with negative carbonate δ^{13}C excursions at the Permian-Triassic boundary: Evidence for upwelling of sulfidic deep-ocean water masses. *Geochemistry Geophysics Geosystems* **9**, Q04025.

Algeo, T.J. & Twitchett, R.J. 2010. Anomalous Early Triassic sediment fluxes due to elevated weathering rates and their biological consequences. *Geology* **38,** 1023–1026.

Arnott, R.W.C., 1993. Quasi-planar-laminated sandstone beds of the Lower Cretaceous Bootlegger Member, north-central Montana: evidence of combined flow sedimentation. *Journal of Sedimentary Petrology* **63**, 488-494.

Beatty, T.W., Zonneveld, J-P. & Henderson, C.M. 2008. Anomalously diverse Early Triassic ichnofossil assemblages in northwest Pangea: A case for a shallow-marine habitable zone. *Geology* **36**, 771-774.

Bond, D.P.G. & Wignall, P.B. 2010. Pyrite framboid study of marine Permo-Triassic boundary sections: a complex anoxic event and its relationship to contemporaneous mass extinction. *Bulletin of the Geological Society of America* **122**, 1265-1279.

Dagis A.A. 1984. Rannetriasovye konodonty severa Srednej Sibiri. (Early Triassic conodonts of northern Middle Siberia.) *Trudy Akademija SSSR*, *Sibirskoe otdelenie Instituta Geologii i Geofiziki* ***554***, 3–69.

Droser, M.L. & Bottjer, D.J. 1986. A semiquantitative field classification of ichnofabric. *Journal of Sedimentary Petrology* **56**, 558-559.

Dumas, S. & Arnott, R.W.C. 1996. Origin of hummocky and swaley cross-stratification – The controlling influence of unidirectional current and aggradation rate. *Geology* **34**, 1073-1076.

Dustira, A.M., Wignall, P.B., Joachimski, M., Blomeier, D., Hartkopf-Fröder, C. & Bond, D.P.G. 2013. Gradual onset of anoxia across the Permian-Triassic boundary in Svalbard, Norway. *Palaeogeography Palaeoclimatology Palaeoecology* **374**, 303-313.

Erwin, D.H. 1993. *The Great Paleozoic Crisis*. Columbia University Press, New York. 327 pp.

Galfetti, T., Hochuli, P.A., Brayard, A., Bucher, H., Weissert, H. & Vigran, J.O. 2007. Smithian-Spathian boundary event: Evidence for global climatic change in the wake of the end-Permian biotic crisis. *Geology* **23**, 291-294.

Grasby, S.E., Beauchamp, B., Embry, A. & Sanei, H. 2013. Recurrent Early Triassic ocean anoxia. *Geology* **41**, 175-178.

Hofmann, R., Buatois, L.A., MacNaughton, R.B. & Mangano, M.G. 2015. Loss of the sedimentary mixed layer as a result of the end-Permian extinction. *Palaeogeography Palaeoclimatology Palaeoecology* **428**, 1-11.

Hofmann, R., Goudemand, N., Wasmer, M., Bucher, H. & Hautmann, M. 2011. New trace fossil evidence for an early recovery signal in the aftermath of the end-Permian mass extinction. *Palaeogeography Palaeoclimatology Palaeoecology* **310**, 216-226.

Horacek, M., Richoz, S., Brandner, R., Krystyn, L. & Spötl, C. 2007. Evidence for recurrent changes in Lower Triassic oceanic circulation in Tethys: The record from marine sections in Iran. *Palaeogeography Palaeoclimatology Palaeoecology* **252**, 355-369.

Isozaki, Y. 1994. Superanoxia across the Permo-Triassic boundary: recorded in accreted deep-sea pelagic chert in Japan. *Memoir of the Canadian Society of Petroleum Geologists* **17**, 805–12.

Isozaki, Y. 1997. Permo-Triassic boundary superanoxia and stratified superocean: records from lost deep sea. *Science* **276**, 235–238.

Jarochowska, E., Tonarová, P., Munnecke, A., Ferrová, L., Sklenář, J. & Vodrážková, A.S., 2013. An acid-free method of microfossil extraction from clay-rich lithologies using the surfactant Rewoquat. *Palaeontologia Electronica* **16**, 7T; 16p.

Knaust, D. 2010. The end-Permian mass extinction and its aftermath on an equatorial carbonate platform: insights from ichnology. *Terra Nova* **22**, 195-202.

Macdonald, H.A., Peakall, J., Wignall, P.B. & Best, J. 2011. Sedimentation in deep-sea lobe elements: implications for the origin of thickening-upwards sequences. *Journal of the Geological Society of London* **168**, 319-332.

Meyer, K.M., Yu, M., Jost, A.B., Kelley, B.M. & Payne, J.L. 2011. $\delta^{13}C$ evidence that high primary productivity delayed recovery from end-Permian mass extinction. *Earth and Planetary Science Letters* **302**, 378-384.

Mørk, A., Embray, A.F. & Weitschat, W. 1989. Triassic transgressive-regressive cycles in the Sverdrup Basin, Svalbard and the Barents Shelf. In *Correlation in hydrocarbon exploration* (ed J.D. Collinson), pp. 113-130. Norwegian Petroleum Society/Graham & Trotman.

Mørk, A., Knarud, R. & Worsley, D. 1982. Depositional and diagenetic environments of the Triassic and Lower Jurassic succession of Svalbard. In *Arctic Geology and Geophysics* (eds. A.F. Embry & H.R. Balkwill). pp. 371-398. Canadian Society of Petroleum Geologists Memoir **8**.

Mørk, A., Elvebakk, G., Forsberg, A.W., Hounslow, M.W., Nakrem, H.A., Vigran, J.O. & Weitschat, W. 1999. The type section of the Vikinghøgda Formation: a new Lower Triassic unit in central and eastern Spitsbergen. *Polar Research* **18**, 51-82.

Mulder, T., Syvitski, J.P.M., Migeon, S., Faugères & Savoye, B 2003. Marine hyperpycnal flows: initiation, behaviour and related deposits. A review. *Marine and Petroleum Geology* **20**, 861-882.

Nakrem, H.A. & Mørk, A. 1991. New early Triassic Bryozoa (Trepostomata) from Spitsbergen, with some remarks on the stratigraphy of the investigated horizons. *Geological Magazine* **128**, 129-140.

Orchard, M.J., 2008. Lower Triassic conodonts from the Canadian Arctic, their intercalibration with ammonoid-based stages and a comparison with other North American Olenekian faunas. *Polar Research* **27**, 393-412.

Payne, J.L., Lehrmann, D.J., Wei, J., Orchard, M.J., Schrag, D.P. & Knoll, A.H. 2004. Large perturbations of the carbon cycle dur- ing recovery from the end-Permian extinction. *Science* **305**, 506–509.

Plink-Björklund, P. & Steel, R.J. 2004. Initiation of turbidity currents: outcrop evidence of hyperpycnal flow turbidites. *Sedimentary Geology* **165**, 29-52.

Pruss, S. B., Fraiser, M. & Bottjer, D. J. 2004. Proliferation of Early Triassic wrinkle structures: implications for environmental stress following the end-Permian mass extinction. G*eology* **32**, 461–464.

Retallack, G.J., Veevers, J.J. & Morante, R. 1996. Global coal gap between Permian-Triassic extinction and Middle Triassic recovery of peat-forming plants. *Bulletin of the Geological Society of America* **108**, 195-207.

Saito, R. Kaiho, K., Oba, M., Takahashi, S., Chen, Z-Q. & Tong, J-N. 2013. A terrestrial vegetation turnover in the middle of the Early Triassic. *Global and Planetary Change* **105**, 152-159.

Song, H-J., Wignall, P.B., Tong, J-N., Bond, D.P.G., Song, H-Y., Lai, X-L., Zhang, K., Wang, H-M. & Chen, Y-L. 2012. Geochemical evidence from bioapatite for multiple oceanic anoxic vents during end-Permian transition with end-Permian extinction and recovery. *Earth and Planetary Science Letters* **353-354**, 12-21.

Song, H-J., Wignall, P.B., Chu, D-L., Tong, J-N., Sun, Y-D., Song, H-Y., He, W-H. & Tian, L. 2014. Anoxia/high temperature double whammy during the Permian-Triassic marine crisis and its aftermath. *Scientific Reports* **4**, 4132, DOI: 10.1038/srep04132.

Sun, Y-D., Wignall, P.B., Joachimski, M.M., Bond, D.P.G., Grasby, S.E., Sun, S., Yan, C.B., Wang, L.N., Chen, Y.L. & Lai, X.L. 2015. High amplitude redox changes in the late Early Triassic of South China and the Smithian-Spathian extinction. *Palaeogeography Palaeoclimatology Palaeoecology* **427**, 62-78.

Sun, Y-D., Joachimski, M.M., Wignall, P.B., Yan, C-B., Chen, Y-L., Jiang H-S., Wang, L-N. & Lai, X-L. 2012. Lethally hot temperatures during the Early Triassic greenhouse. *Science* **388**, 366-370.

Tian, L., Tong, J-N., Algeo,, T.J., Song, H-J., Song, H-Y., Chu, D-L., Shi, L. & Bottjer, D.J. 2014. Reconstruction of Early Triassic ocean redox conditions based on framboidal pyrite from the Nanpanjiang Basin, South China. *Palaeogeography Palaeoclimatology Palaeoecology* **412**, 68-79.

Wignall, P.B., Bond, D.P.G., Kuwahara, K., Kakuwa, K., Newton, R.J. & Poulton, S.W. 2010. An 80 million year oceanic redox history from Permian to Jurassic pelagic sediments of the Mino-Tamba terrane, SW Japan, and the origin of four mass extinctions. *Global and Planetary Change* **71**, 109-123.

Wignall, P.B. & Hallam, A. 1992. Anoxia as a cause of the Permian/Triassic extinction: facies evidence from northern Italy and the western United States. *Palaeogeography, Palaeoclimatology, Palaeoecology* **93,** 21-46.

Wignall, P.B., Morante, R. & Newton, R. 1998. The Permo-Triassic transition in Spitsbergen: $\delta^{13}C_{org.}$ chemostratigraphy, Fe and S geochemistry, facies, fauna and trace fossils. *Geological Magazine*, **133**, 47-62.

Wignall, P.B. & Newton, R. 1998. Pyrite framboid diameter as a measure of oxygen deficiency in ancient mudrocks. *American Journal of Science* **298,** 537-552.

Wignall, P.B. & Newton, R. 2001. Black shales on a basin margin: a model based on examples from the Upper Jurassic of the Boulonnais, northern France. *Sedimentary Geology* **144**, 335-356.

WIGNALL, P.B. & TWITCHETT, R.J. 2002. Extent, duration and nature of the Permian-Triassic superanoxic event. In *Catastrophic events and mass extinctions: impacts and beyond.* (eds. Koeberl, C. & MacLeod, K. C.). pp. 395-413. Geological Society of America Special Paper **356**.

WILKIN, R.T., BARNES, H.L. & BRANTLEY, S.L., 1996, The size distribution of framboidal pyrite in modern sediments: An indicator of redox conditions. *Geochimica et Cosmochimica Acta* **60**, 3897–3912.

YAN, C.B., WANG, L.N., JIANG, H.S, WIGNALL, P.B., SUN, Y.D., CHEN, Y.L. & LAI, X.L., 2013. Uppermost Permian to Lower Triassic Conodonts at Bianyang Section, Guizhou Province, South China. *Palaios* **28**, 509-522.

ZONNEVELD, J-P., GINGRAS, M.K. & BEATTY, T.W. 2010. Diverse ichnofossil assemblages following the P-T mass extinction, Lower Triassic, Alberta and British Columbia: evidence for shallow marine refugia on the northwestern coast of Pangea. *Palaios* **25**, 368-392.

Figure 1


100 km
Kvitøya
Nordaustlandet
Spitsbergen
Kong Karls Land
Barentsøya
Edgeøya
Nord-
fjorden
Tschermakfjellet
Isfjorden
Vindodden
Festningen
V. Mijenfjorden
Forkastningsdalen

Figure 2

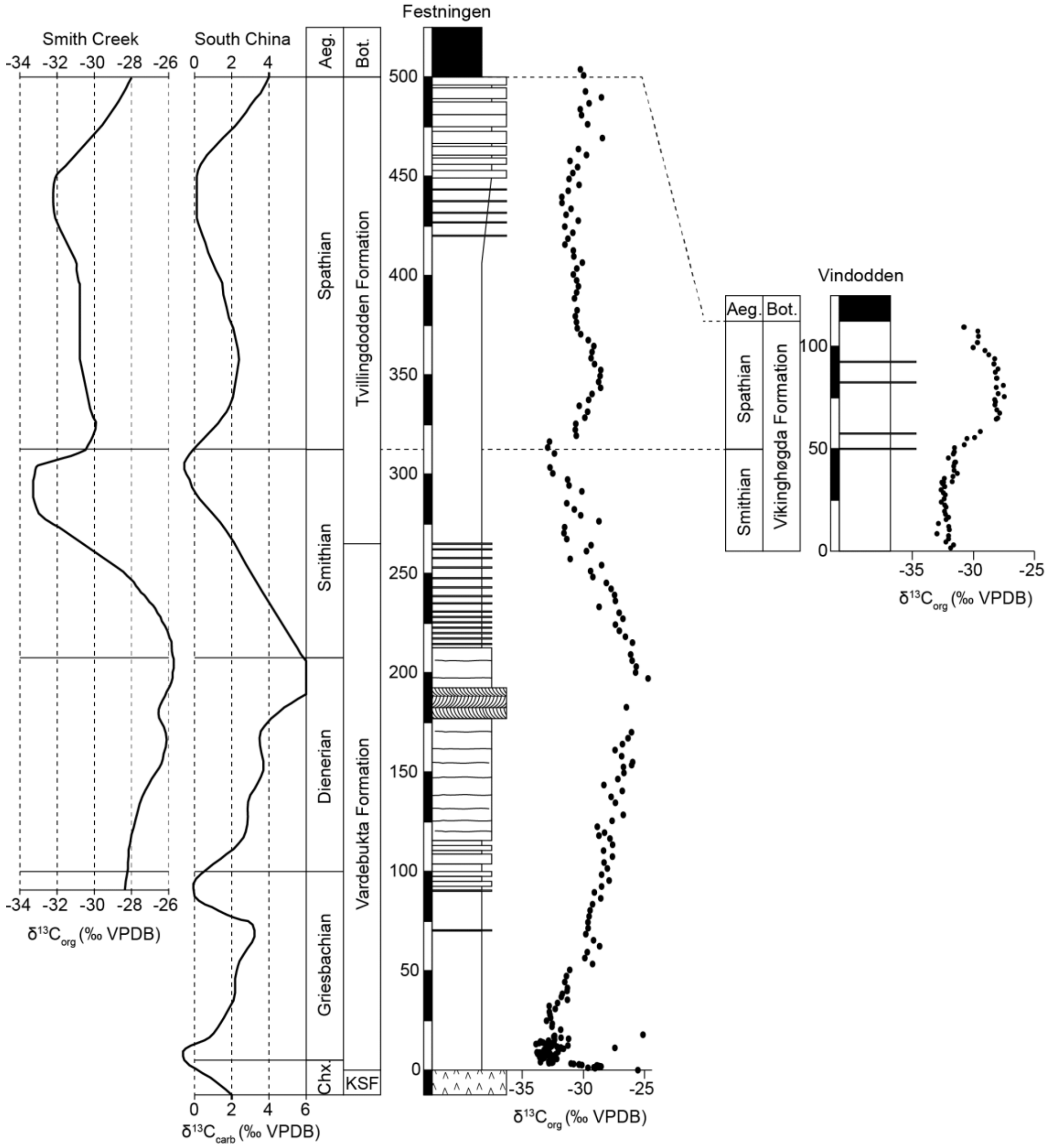
Smith Creek
South China
Aeg.
Bot.
Festningen
Spathian
Smithian
Dienerian
Griesbachian
Chx.
KSF
Tvillingodden Formation
Vardebukta Formation
δ13Corg (‰ VPDB)
δ13Ccarb (‰ VPDB)
Vindodden
Vikinghøgda Formation
-34 -32 -30 -28 -26
0 2 4 6
500 450 400 350 300 250 200 150 100 50 0
-35 -30 -25

Figure 3

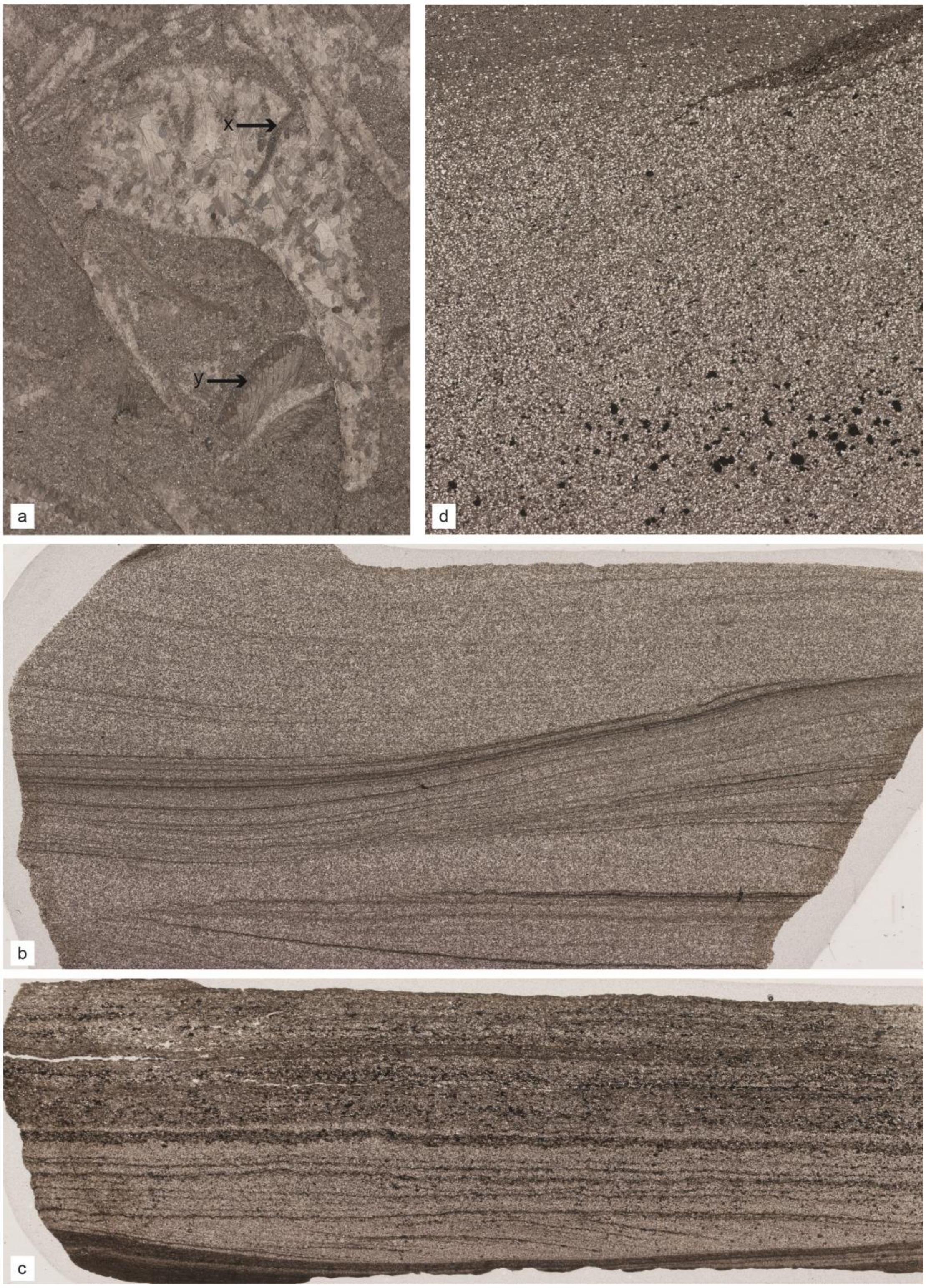

Figure 5

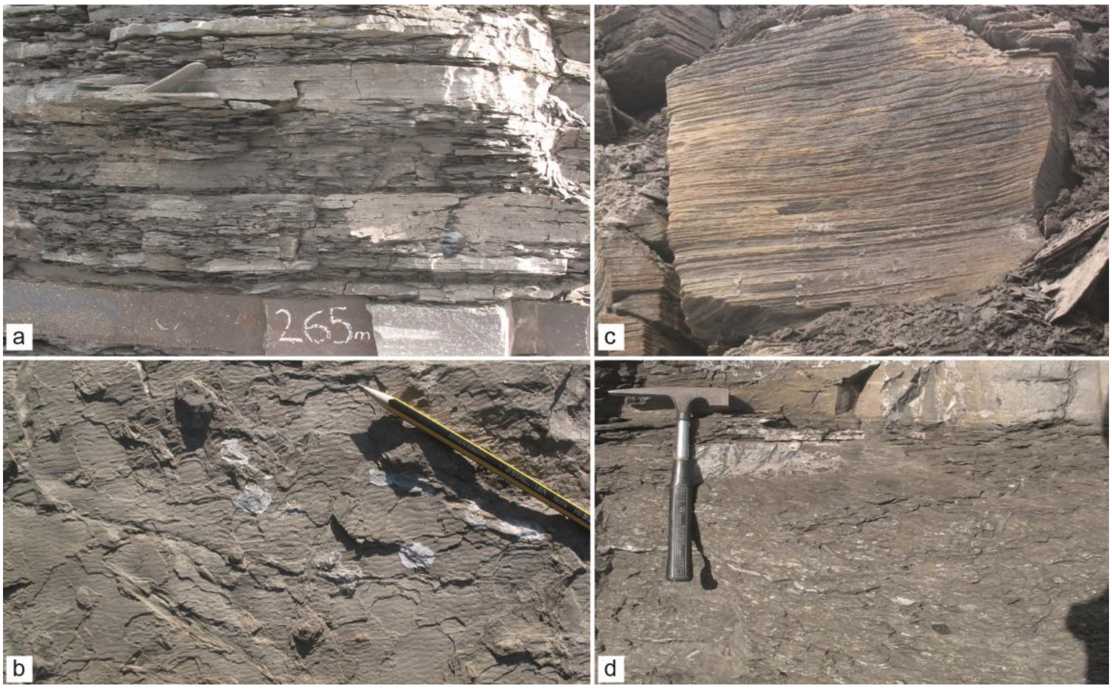

Figure 6

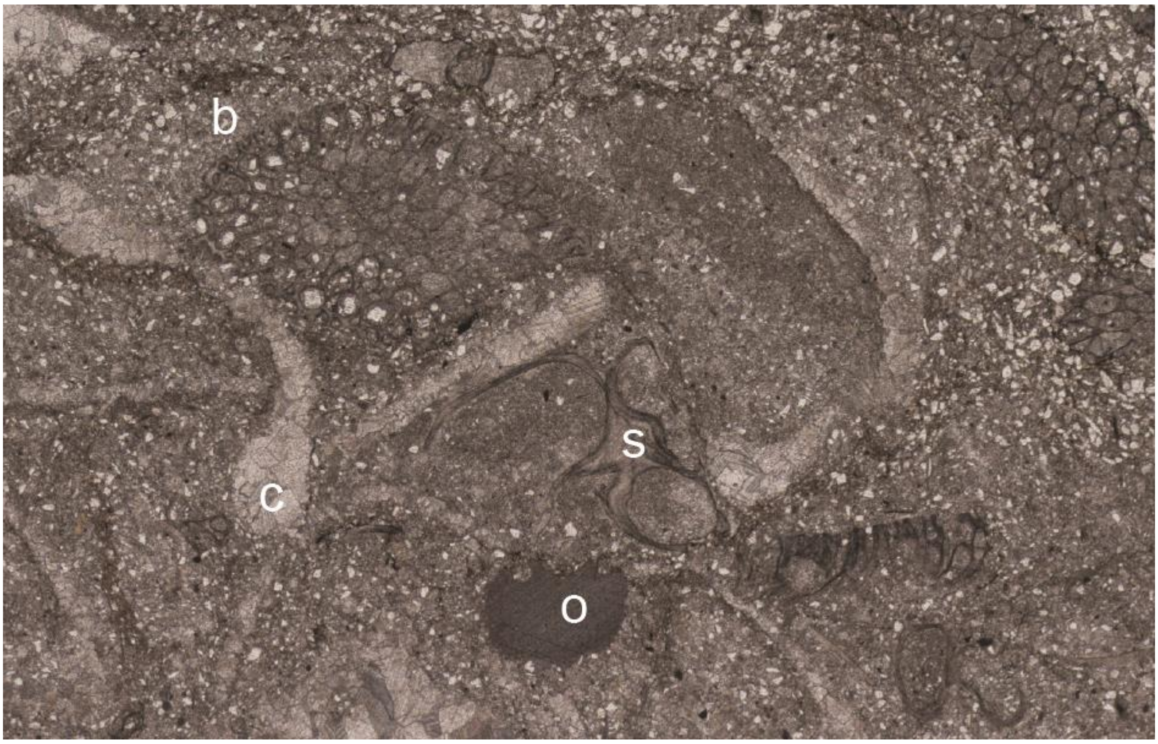

Figure 7


FESTNINGEN
FORKASTNINGSDALEN
Anoxic phases
Ichnofabric index
metres
IV
III
II
?
c si fs
1 2 3 4 5 6
P
W
Ich. Index
KEY
W Wrinkle marks
P Promyalina
Wave ripples
Flame structures
Escape burrows
Climbing ripples
Current ripples
Bivalves

Figure 8

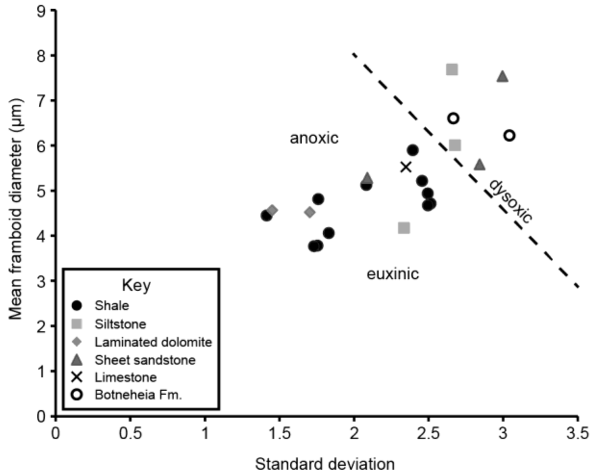

anoxic
euxinic
dysoxic
Key
Shale
Siltstone
Laminated dolomite
Sheet sandstone
Limestone
Botneheia Fm.
Mean framboid diameter (µm)
Standard deviation
0
1
2
3
4
5
6
7
8
9
0.5
1.5
2.5
3.5

Figure 9

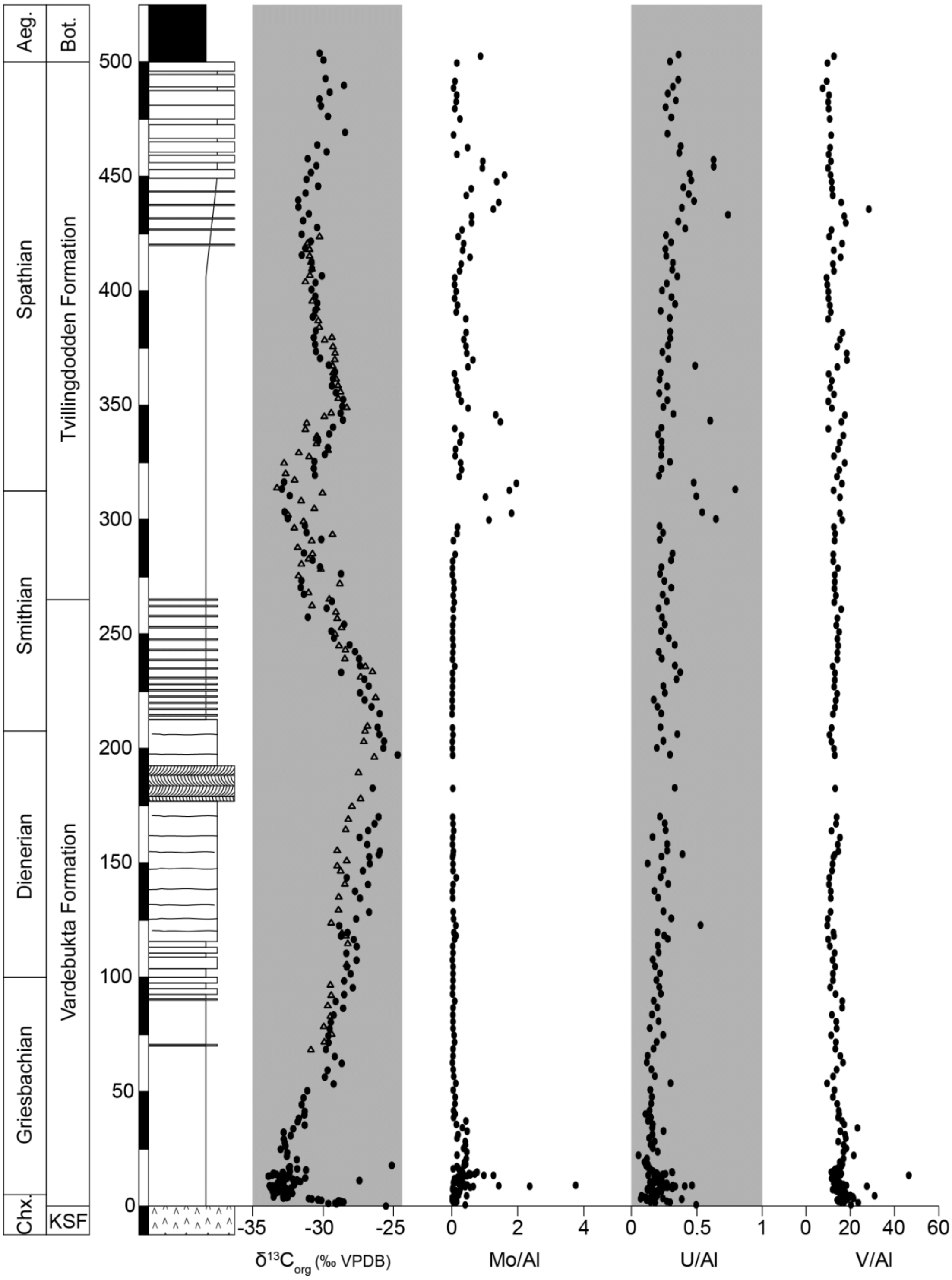

Aeg.
Bot.
Spathian
Smithian
Dienerian
Griesbachian
Chx.
Tvillingodden Formation
Vardebukta Formation
KSF
0
50
100
150
200
250
300
350
400
450
500
-35
-30
-25
δ¹³C_org (‰ VPDB)
0
2
4
Mo/Al
0
0.5
1
U/Al
0
20
40
60
V/Al

Figure 10

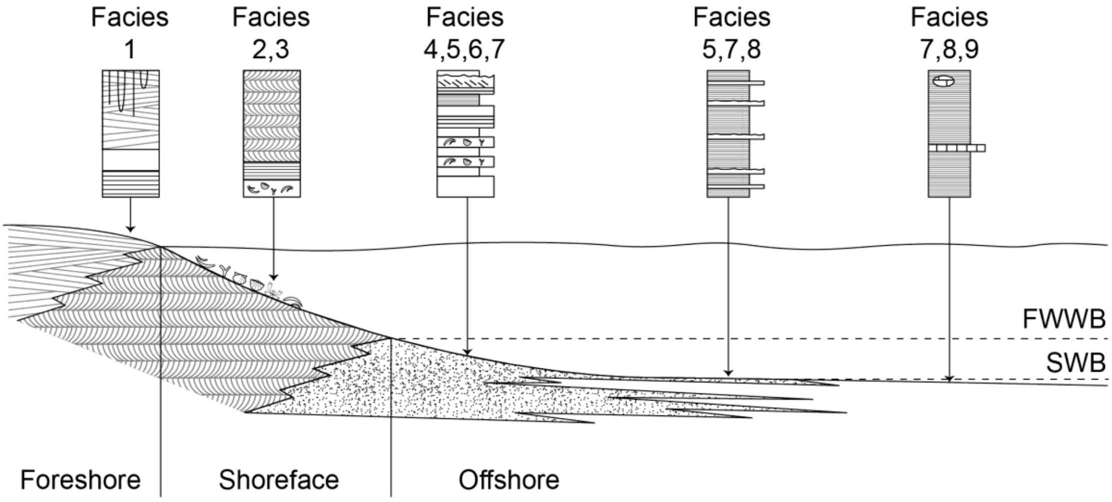
Facies
1
Facies
2,3
Facies
4,5,6,7
Facies
5,7,8
Facies
7,8,9
FWWB
SWB
Foreshore
Shoreface
Offshore

Figure 11

844

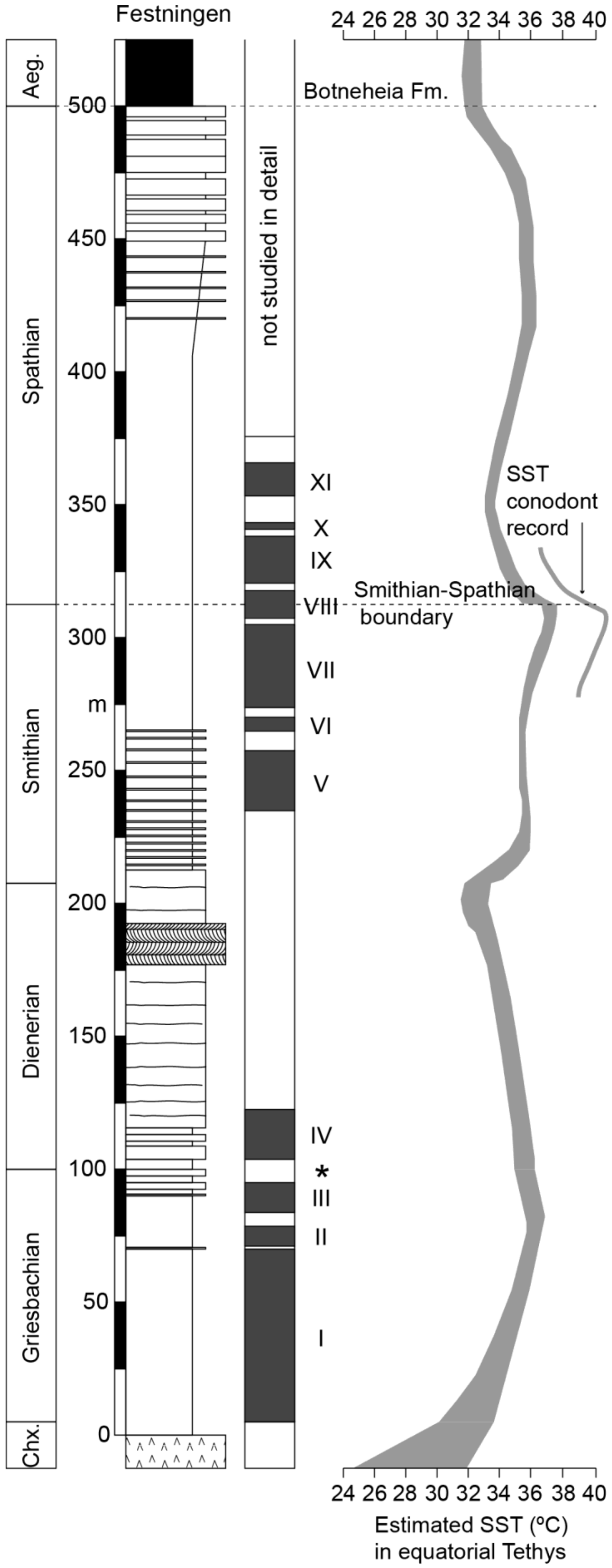

Festningen
Aeg.
Spathian
Smithian
Dienerian
Griesbachian
Chx.
500
450
400
350
300
m
250
200
150
100
50
0
not studied in detail
Botneheia Fm.
XI
X
IX
VIII
VII
VI
V
IV
*
III
II
I
SST
conodont
record
Smithian-Spathian
boundary
24 26 28 30 32 34 36 38 40
Estimated SST (ºC)
in equatorial Tethys

845